Department of Physics and Astronomy
University of Heidelberg

Bachelor Thesis in Physics
submitted by

Darius Hoffmann

born in Mannheim (Germany)

2015

The Transition to Chaos in the two-dimensional Bose-Hubbard Model

ii

This Bachelor Thesis has been carried out by Darius Hoffmann at the
Institute for Theoretical Physics in Heidelberg
under the supervision of
Dr. Sandro Wimberger

ABSTRACT

In this thesis we investigate the spectra of the 2D Bose-Hubbard Hamiltonian which can be used to describe an ultracold dilute gas of bosonic atoms in an optical lattice. The spectra are numerically calculated and, taking symmetries into account, a level statistical analysis is performed. This is done on a number of different small 2D systems in order to analyze the transition of regular systems into quantum chaotic systems as characterized by their spectral properties.

ZUSAMMENFASSUNG

Gegenstand dieser Arbeit ist eine Untersuchung der Spektren des 2D Bose-Hubbard Hamiltonian, welcher zur Beschreibung eines ultrakalten, stark verdünnten Bosonengases genutzt werden kann. Die Spektren werden numerisch berechnet und unter Berücksichtigung der Symmetrien statistisch untersucht. Wir betrachten eine Reihe verschiedener kleiner 2D Systeme in der Absicht einer Analyse des Übergangs von regulären zu chaotischen Quantensystemen, welche jeweils durch repräsentative Eigenschaften der Spektren charakterisiert sind.

CONTENTS

Part I

INTRODUCTION

Among other aspects the first realizations of Bose-Einstein condensates and the great interest this brought on, led to the development of an impressive array of methods and techniques in cooling and controlling atoms. Of particular interest to the study of quantum chaos are setups of ultracold bosons stored in optical lattices because of the immense control achievable through optical methods and the variety of different systems engineerable [7],[11]. They can be described in a tight-binding approximation known as the Bose-Hubbard model which is especially well suited to describe systems with sufficiently deep lattices sites since the intra-well dynamics are neglected [11],[3]. In classical systems regular and chaotic motion have long been recognized and understood but only in more recent years was chaos in quantum systems systematically investigated and the concept expanded to systems without clear classical counterpart. An important step in this achievement are the ideas of random matrix theory introduced by Wigner, which hold independently of the specific system, and allow a characterization of the system through its spectral properties [18],[12]. In the article [1] the 1D Bose-Hubbard Model was first shown to exhibit quantum chaos in its spectral statistics and there have been many studies of quantum chaos in all its aspects in the 1D model since [16],[17],[5]. However, to the best of our knowledge, non concerning the transition to chaos in the 2D Bose-Hubbard model, we therefore endeavor to provide a step towards a better understanding of these systems in this numerical study of small 2-dimensional systems.

THEORY

In this section a brief overview and some references of the most important theoretical aspects of the subject at hand are given. First the Bose-Hubbard model is introduced followed by a short preface to the concept of quantum chaos primarily focused on the statistical approach.

1.1 BOSE-HUBBARD MODEL

The Hubbard Model is a simple theoretical model, introduced in 1963 by John Hubbard, used to describe systems of interacting electrons in a lattice using in a tight-binding approximation [10]. An adapted version of the model can describe bosons as well with different commutator relations for the creation and annihilation operators [7],[11],[3]. In an optical lattice the confining potential is realized via lasers creating a standing wave of depth V_0. Thus the potential can be described by

$$V(x) = V_0\, sin^2(kx) \tag{1}$$

On such a lattice the effective Hamiltionian investigated is given by

$$\hat{H}_{BHM} = -J \sum_{\langle i,j \rangle} \hat{a}_i^\dagger \hat{a}_j + \frac{U}{2} \sum_{i=1}^{L} \hat{a}_i^\dagger \hat{a}_i^\dagger \hat{a}_i \hat{a}_i \tag{2}$$

where L represents the number of lattice sites and $\langle i,j \rangle$ indicates that the sum is to be taken over all pairs of neighboring sites i,j. The operators $\hat{a}_i^\dagger$ and $\hat{a}_i$ are the boson creation and annihilation operators on Fock states with the well known operator identities

$$[\hat{a^\dagger}_i, \hat{a}_j^\dagger] = [\hat{a}_i, \hat{a}_j] = 0 \tag{3}$$

$$[\hat{a}_i, \hat{a}_j^\dagger] = \delta_{ij} \tag{4}$$

In the Hamiltonian the first term, the *hopping term*, allows for the tunneling of bosons to neighboring wells and the parameter J is the hopping matrix element. The second term describes the interactions of particles in the same lattice site, so for $U > 0$ the parameter U represents the strength of a repulsive on site interaction. The one-particle eigenstates in this standard model are the highly localized *Wannier functions* which justifies considering only the tunneling to directly adjacent lattice sites and neglecting intra-well dynamics, i.e. expecting all particles in a well to be in the ground state. Experimentally this model is approximated by a sufficiently deep lattice.
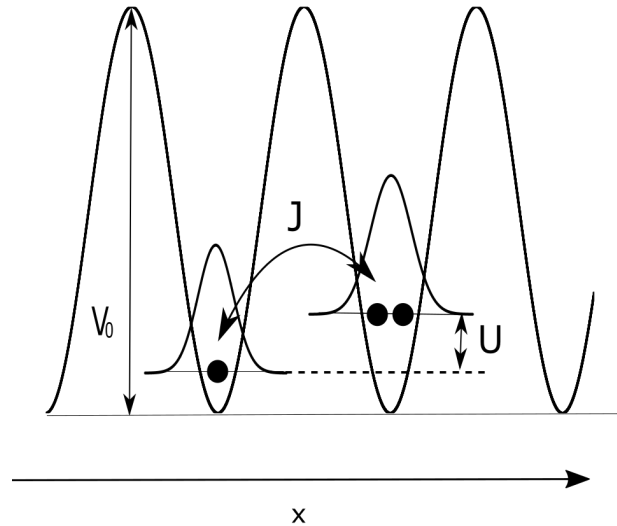
Figure 1: Illustration of the parameters in the Hamiltonian

1.2 QUANTUM CHAOS AND RANDOM MATRIX THEORY

A classical system is said to be chaotic if it is nonintegrable, i.e. the number of degrees of free-dom exceeds the number of constants of motion, and highly sensitive to initial conditions in the sense that the distance of the trajectories of two initially nearby points in phase space grows exponentially in time. In applying this concept of sensitivity to initial conditions to quantum systems one cannot simply consider the scalar product of to slightly different wave functions with the same Hamiltonian since it is constant due to the unitarity of the time evolution oper-ator. Instead the evolution of two initially identical states under slightly varied Hamiltonians need to be considered. This approach allows for a characterization of chaotic systems through the systems dynamics [18, 6].

The other property of classically chaotic systems, its nonintegrability, can also be expanded to quantum systems. A quantum system is integrable if there are as many quantum numbers as there are degrees of freedom. It follows that in an integrable system the energy levels are all independent of each other. As mentioned the statistical properties of the energy levels also enable to characterize the system by comparison to the predictions of random matrix theory for regular and chaotic systems and this fundamental approach of statistical analysis is adopted in this study. The two concepts are related through the spectral theorem stating that the time evolution operator is always expandable in the basis of eigenenergies of the Hamiltonian. The *avoided crossing theorem* in perturbation theory tells us that if states are coupled the levels will repel each other as the strength of the perturbation is varied, usually by a control parameter in the Hamiltonian, i.e. a crossing of the energy levels is avoided [13]. In contrast in a regular, integrable system the energy levels are independent so there is no repulsion of levels. Therefore the idea of random matrix theory, in short RMT, is to study the fluctuations of level distances as they convey something about the probability of crossing or anti-crossing of levels, thereby characterizing the system as regular, chaotic or mixed [18, 6, 12, 15].

1.2.1 *Irreducible Representation of the Hamiltonian-Matrix*

Before analyzing the spectrum of a given Hamiltonian-Matrix the symmetries of a system need to be taken into account. Given an operator $\hat{S}$ representing a symmetry of the system, i.e.

$$[\hat{S}, \hat{H}] = 0 \tag{5}$$

a common eigenbasis $|m, n\rangle$ of $\hat{S}$ and $\hat{H}$ can be found and the Hamiltonian-Matrix in this basis is of block-diagonal form:

$$\langle m', n' | \hat{H} | m, n \rangle = \delta_{m,m'} H^{(m)}_{n,n'} \tag{6}$$

The size of the respective blocks is then determined by the degeneracy of the eigenvalues s_m of $\hat{S}$ and the subsystems defined by the blocks do not couple. Therefore, if there are more symmetries present each block can be treated separately with the same procedure leading to an *Irreducible Representation of the Hamiltonian-Matrix* if there are no further symmetries. The blocks then must be analyzed independently for a representative picture of the energy level fluctuations. This avoids a mixing of the blocks which can lead to degeneracies not present in the separated blocks [18].

1.2.2 *Unfolding of the Spectrum*

Given the spectrum of a block of the Hamiltonian-Matrix in its irreducible representation the level density $\rho(E)$ can be decomposed into a smooth part and a rapidly oscillating part. The smooth part gives the system specific global trend and since we are mainly interested in the locally fluctuations we need to renormalize the spectrum in order to reduce the information contained to the local fluctuating part. This process, which is usually referred to as *unfolding of the spectrum* is generally done as follows [18, 9]:

1. Sorting the N eigenenergies of a block in ascending order:
   $E_0 \leq E_1 \leq E_2 \leq \ldots \leq E_N$

2. Calculating the *staircase function* $N(E)$ giving the number of energy levels up to energy E

3. Approximating the staircase function by a smooth function $\overline{N}(E)$

4. Determining the new unfolded, dimensionless levels ϵ_i as
   $\epsilon_i = \overline{N}(E_i)$, thereby creating a local density of states of approximately one

1.2.3 *Nearest Neighbor Statistics*

Such an unfolded spectrum can now be analyzed statistically and characterized. The most common way to do so is through its *nearest neighbor statistics*. One calculates the distances between unfolded levels $s_i = \epsilon_{i+1} - \epsilon_i$ and compares the distribution of these level spacings with the predictions of random matrix theory for regular/chaotic systems in the limit of a level continuum [18].
The following statements can be derived exactly for ensembles of random 2x2 matrices and it
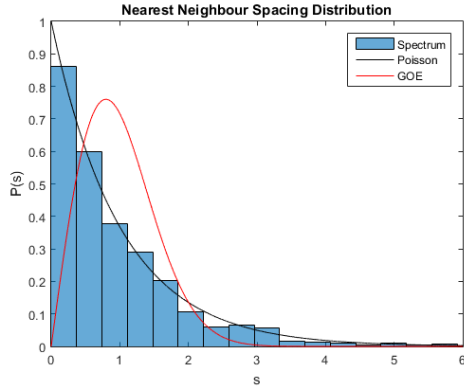
Figure 2: Example for a spacing distribution approximately Poission distributed. Data taken form our calculations, details following.
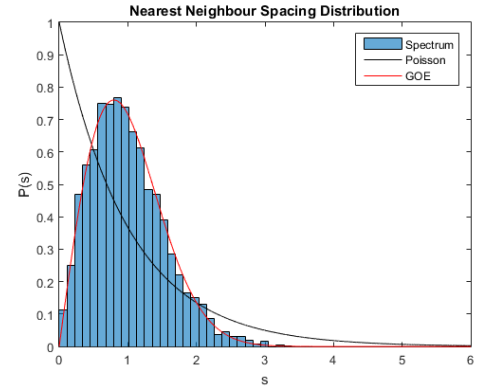

Figure 3: Example for a spacing distribution approximately GOE distributed. Data taken form our calculations, details following.

is the so called *Wigner surmise* that they hold for the general case of NxN matrices. Assuming a random distribution of ordered, real numbers, as is to be expected in the case of an integrable system with independent energy levels, the probability density of finding a level within a distance s form another is expected to be Poisson distributed, i.e. $P(s) = e^{-s}$, in the continuous limit. The spectra of chaotic systems have been found to correspond to predictions for certain ensembles of random matrices. In the given case of a real Hamiltonian random matrix theory predicts the spacings to correspond to the Gaussian orthogonal ensemble (GOE), i.e. a spacing distribution $P(s) = s\frac{\pi}{2}e^{-s^2\frac{\pi}{4}}$ in the continuous limit. In the latter case the spacings are also said to be Wigner-Dyson (WD) distributed [18, 15].

Part II

METHODS AND ANALYSIS

METHODS

2.1 NUMERICAL IMPLEMENTATION OF THE SYSTEM

This section details the numerical implementation of the system using Matlab. Specificly the construction of the Fock-Basis for an arbitrary number of lattice sites L and particle number N as well as the calculation of the matrix representation of the Hamiltonian in this basis will be described. For clarification code excerpts are provided where helpful or necessary.

2.1.1 Construction of the Fock-Basis

Taking the number of lattice sites L and particle number N as input a simple function for the construction of a matrix B where the columns correspond to the lattice sites 1 through L and the rows form the different Basis vectors, i.e. $B(n, m)$ gives the occupation number of the m'th lattice site in the n'th basis state, was implemented as follows.

1. Constructing a matrix with rows containing all combinations of L integers $n_1, n_2 \ldots, n_L$ form the set $\{0, 1, \ldots, N\}$.

```
1  ct=1;
2  for i=1:L
3      if i==1
4        inpt=(0:N);
5      else
6        inpt=[inpt,(0:N)];
7        ct=ct+L;
8      end
9  end
10
11 comb = combnk(input,L);
12
13 A=unique(comb,'rows');
```

2. Sorting out rows with $\sum_{i=1}^{L} n_i \neq N$ leaves the desired matrix.

```
1  idx = ( sum(A,2)==N );
2  B=A(idx,:)
```

The dimension of the Hilbert space is easily derived form combinatorial considerations and reads

$$dim(\mathcal{H}) = \binom{L + N - 1}{N} \tag{7}$$

2.1.2   *Construction of the Hamiltonian-Matrix in the Fock-Basis*

To construct the Hamiltonian-Matrix in the established Fock-Basis we first need to specify what the general system described looks like. For generality and flexibility we consider an $M_i \times M_j$ lattices with $L = M_i \cdot M_j$. A lattice site and nearest neighbors are coupled by the hopping term in equation (2). To include hopping to diagonally neighboring lattice sites with flexibility as to which sites are diagonally coupled and the strength of the coupling we include another hopping term with an independent parameter J_d and the diagonally coupled sites specified in a set DC (see fig. 4):

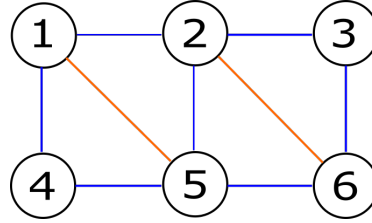$$-J_d \sum_{(i,j) \in DC} \hat{a}_i^\dagger \hat{a}_j \tag{8}$$

Figure 4: Visualization of a 2x3 System where the circles represent the lattice sites, and the lines couplings of the sites, i.e. blue lines represent a nearest neighbor coupling with J and orange lines a diagonal coupling with J_d, so here DC={(1,5),(2,6)}.

Analytically the creation and annihilation operators act on Fock-states like

$$\hat{a}_i^\dagger \left| n_1, \ldots n_r \ldots \right\rangle = \sqrt{n_r + 1} \left| n_1, \ldots n_r + 1 \ldots \right\rangle \tag{9}$$

and

$$\hat{a}_i \left| n_1, \ldots n_r \ldots \right\rangle = \sqrt{n_r} \left| n_1, \ldots n_r - 1 \ldots \right\rangle \tag{10}$$

Therefore for the on-site interaction it holds that

$$\frac{U}{2} \sum_{i=1}^{L} \hat{a}_i^\dagger \hat{a}_i^\dagger \hat{a}_i \hat{a}_i \left| n_1, n_2, \ldots, n_L \right\rangle = \frac{U}{2} \sum_{i=1}^{L} n_i(n_i - 1) \left| n_1, n_2, \ldots, n_L \right\rangle \tag{11}$$

and the hopping terms give

$$-J/J_d \sum_{\langle i,j \rangle / (i,j) \in DC} \hat{a}_i^\dagger \hat{a}_j \left| n_1, \ldots, n_i, \ldots, n_j, \ldots \right\rangle$$
$$= -J/J_d \sum_{\langle i,j \rangle / (i,j) \in DC} \sqrt{n_i + 1} \sqrt{n_j} \left| n_1, \ldots, n_i + 1, \ldots, n_j - 1, \ldots \right\rangle \tag{12}$$

For the numerical calculation of the matrix elements we compute the contributions of the separate terms individually:

1. On-Site Interaction:

   Since applying the creation and annihilation operators to the same state leaves the state unchanged exept for additional coefficients, see (11), the calculation of a matrix element $\frac{U}{2} \sum_{i=1}^{L} \langle n_1^{(k)}, n_2^{(k)}, \ldots, n_L^{(k)} | \hat{a}_i^\dagger \hat{a}_i^\dagger \hat{a}_i \hat{a}_i | n_1^{(l)}, n_2^{(l)}, \ldots, n_L^{(l)} \rangle$ is easily implemented with a comparison of the basis vectors k and l and in case of equality starting a loop $i = 1$ to L summing up the factors $\sum_{i=1}^{L} n_i (n_i - 1)$ and finally multiplying the result with $\frac{U}{2}$.

2. Nearest Neighbor Hopping:
   Constructing a matrix P with rows containing all pairs of nearest neighbors is easy enough and taking P as input a matrix element
   $J \sum_{\langle i,j \rangle} \langle n_1^{(k)}, n_2^{(k)}, \ldots, n_L^{(k)} | \hat{a}_i^\dagger \hat{a}_j | n_1^{(k)}, n_2^{(l)}, \ldots, n_L^{(l)} \rangle$ was calculated as follows.
   Given equation (11) a summand only contributes if
   $\delta_{n_1^{(k)}, n_1^{(l)}} \delta_{n_2^{(k)}, n_2^{(l)}} \ldots \delta_{n_i^{(k)}, n_i^{(l)}+1} \ldots \delta_{n_j^{(k)}, n_j^{(l)}-1} \ldots = 1,$

   therefore, in a loop going through all pairs of nearest neighbors, as first step, we compare the occupation numbers in the basis vectors k and l for the sites unequal the coupled pair:

```
m=0;
sze=size(P);

for i=1:sze(1)
    r=l;
    r(P(i,1))=0;
    r(P(i,2))=0;

    s=k;
    s(P(i,1))=0;
    s(P(i,2))=0;

    if r==s
```

   and in case of equality $\delta_{n_i^{(k)}, n_i^{(l)}+1} \delta_{n_j^{(k)}, n_j^{(l)}-1} = 1$ is implemented for (i,j) and (j,i) by a direct comparison of the occupation numbers, after the application of the operators, i.e. of either a tunneling $i \longrightarrow j$ or $j \longrightarrow i$ and eventually the contribution added

```
    if l(P(i,1))-1==k(P(i,1)) & l(P(i,2))+1==k(P(i,2))
        m=m-(sqrt(l(P(i,1)))*sqrt(l(P(i,2))+1));
    elseif l(P(i,1))+1==k(P(i,1)) & l(P(i,2))-1==k(P(i,2))
        m=m-(sqrt(l(P(i,1))+1)*sqrt(l(P(i,2))));
    end
    end
end
```

   Finaly multiplication with the Parameter J gives the matrix element.

3. Diagonal Neighbor Hopping:
   The same algorithm used to calculate the nearest neighbor hopping contributions to a given matrix element can of course be applied to account for diagonal hopping of particles by simply taking as input-matrix P the combinations of diagonally coupled pairs specified in the set DC and multiplication with the parameter J_d in the last step.

2.2   TRANSFORMATION TO THE IRREDUCIBLE REPRESENTATION

To transform the Fock-Basis and Hamiltonian-Matrix in Fock-Basis to the latters irreducible representation, as explained in 1.2.1, we first need to identify the systems symmetries. Then we have to go over all symmetries to find common eigenbases of all operators already involved in the separation of the symmetry reduced subspaces represented by the blocks in the respective block-diagonal representations.

2.2.1   *Identifying Symmetries*

To identify the symmetries we employ a brute-force method of checking all possible permutations of the lattice sites for symmetries by calculating the commutator of the Hamiltonian and the respective permutation operators.
   The implementation is done as follows.

1. Establishing all permutations and starting a loop.

```
1  Perms=perms(1:L);
2  sizeperms=size(Perms);
3  for permct=1:sizeperms(1);
```

2. Calculating the permutated basis vectors for a given permutation.

```
1  idx = [Perms(permct,:)];
2  B_perm=B(:,idx);
```

3. Setting up the permutation operator in Fock-Basis using two loops.

```
1  for k_b=1:s(1)
2    for l_b=1:s(1)
3       if B(k_b,:)==B_perm(l_b,:)
4           P_perm(k_b,l_b)=1;
5       end
6    end
7  end
```

4. Computing the commutator as

```
1  komm_H_P_perm=(H*P_perm)-(P_perm*H);
```

with the Hamiltonian-Matrix set up as in 2.1.2 and in case it vanishes putting the current permutation on a list.

While this is certainly a very crude method for the systems under consideration going up to L=9 it is just efficient enough since it needs to be performed once per specific system and can be applied with N=2 keeping the dimension as small as possible.

2.2.2 *Constructing the Basis for the irreducible Representation*

To construct the basis for the irreducible representation of the Hamiltonian we use a loop going over all symmetries identified. Inside the loop a function going through all blocks in the current representation, checks if the basis of the respective subspaces can be transformed into an eigenbasis of the symmetrieoperator under consideration and if so calculates the new basis vectors and blockconfiguration.

As input the funktion takes the coefficients of the basis vectors computed in the previous iteration in the Fock-Basis collected as rows in a matrix B_{coeff} and the configuration of blocks as a vector *blockconfig* containing entries giving the size of the current blocks as well as the permutation giving the symmetry and other quantities computed prior. B_{coeff} and blockconfig are updated in every iteration and the starting values are of course the identity matrix $\mathbb{1}_{dim(\mathcal{H})}$ for the basis coefficients and a 1×1 vector with the entry $dim(\mathcal{H})$.

Step by step the function proceeds as follows.

1. First the representation of the symmetry permutation in the current Basis is computed for all blocks and saved in an array. Analogous to the steps 2 and 3 in the identification of the symmetries a matrix P_{perm} is set up and the matrix representation of the symmetry operator in the separate blocks computed by the corresponding matrix multiplication.

```
1  sizeconfig=size(blockconfig);
2  bstepper=0;
3  for t=1:sizekonfig(2)
4
5      Pij{t}=conj(B_koeff(1+bstepper:blockconfig(t)+bstepper,:))*transpose(B_koeff(1+
           bstepper:blockconfig(t)+bstepper,:)*transpose(P_perm));
6
7      bstepper=bstepper+blockconfig(t);
8  end
```

2. Then the eigenvalue problem is solved for all the matrices in the array using Matlabs *eig()* function.

```
1  for t2=1:sizeconfig(2)
2
3  [EVPij,EWPij_num] = eig(Pij{t2},'vector');
4
5      EWPij=round(EWPij_num,6);
6
7      newewblksunsrtd{tu}=EWPij;
8      newevblksunsrtd{tu}=EVPij;
9  end
```

3. It is checked which blocks decompose into smaller blocks by testing whether all eigenvalues have absolute value one and there are more than one different eigenvalue.

4. For the blocks that break down the corresponding eigenvectors are sorted so eigenvectors with the same eigenvalue are grouped together and the updated blockconfiguration is set up accordingly.

5. Finally the new basis coefficients are calculated by going through all blocks that decompose and computing the new coefficients corresponding to the grouped eigenvalues as scalar product of the eigenvectors and corresponding old basis coefficients. That means the eigenvectors found in the current basis are expressed in the Fock-Basis by calculating

$$
\begin{aligned}
\vec{d}^{(i)} * \begin{pmatrix} C_1 \\ C_2 \\ \vdots \\ C_z \end{pmatrix} &= d_1^i C_1 + d_2^i C_2 + \dots \\
&= d_1^{(i)} \sum_k a_k^{(1)} |n_1^{(k)}, n_2^{(k)}, \dots\rangle \\
&\quad + d_2^{(i)} \sum_k a_k^{(2)} |n_1^{(k)}, n_2^{(k)}, \dots\rangle \\
&\qquad\qquad\qquad \vdots \\
&= (d_1^{(i)} a_1^{(1)} + d_2^{(i)} a_1^{(2)} + \dots) |n_1^{(1)}, n_2^{(1)}, \dots\rangle \\
&\quad + (d_1^{(i)} a_2^{(1)} + d_2^{(i)} a_2^{(2)} + \dots) |n_1^{(1)}, n_2^{(1)}, \dots\rangle \\
&\qquad\qquad\qquad \vdots
\end{aligned}
\tag{13}
$$

where $\vec{d}^{(i)}$ represents one eigenvector in the subspace/block currently given by the basis $\{C_1, \dots, C_z\}$, for all eigenvectors and exchanging the new coefficients in the corresponding place in B_{coeff}.

2.2.3 *Transforming the Hamiltonian-Matrix to the irreducible Representation*

Given the basis for the irreducible representation represented by the matrix B_{coeff} calculated in the last iteration of the algorithm discussed in the previous section, a simple basis transformation giving the irreducible representation was implemented as a matrix multiplication.

```
1  H_irred=B_koeff*H*conj(transpose(B_koeff));
```

2.3 UNFOLDING AND STATISTICAL TESTS

2.3.1 *Unfolding and Nearest Neighbor Spacings*

For the calculation of the unfolded level spacings we perform what is known as *local unfolding* [9]. The mean level density is assumed to be approximately linear in a window of w levels on

each side of two neighboring sorted energies E_i, E_{i+1}. The unfolded spacings are then computed directly as

$$s_i = \overline{\rho_L}\,(E_{i+1} - E_i) = \frac{2w + 1}{E_{i+w+1} - E_{i-w}}\,(E_{i+1} - E_i) \tag{14}$$

The window defined by w must be big enough to smooth the local density and obtain a good approximation of local density one but also small enough in order not to average to much the fluctuations we are interested in [18]. We generally found this to be realized well for $w \approx 6$.

2.3.2 *Further statistical Tests*

To quantify the agreement of the calculated spacing distributions with the predictions for regular and chaotic systems and to be able to compare the findings for a series of different parameters we perform a χ^2 like test computed as follows [17].

The spacings are binned for a number of bins $N_{bin} \in [15, 35]$ and the quantity

$$\chi^2 = \sum_i^{N_{bin}} \frac{(P(b_i) - P(b_i)_{rmt})^2}{P(b_i)_{rmt}} \tag{15}$$

where the b_i represent the bins and $P(b_i)$ the probabilities, is calculated. The theoretical probabilities $P(b_i)_{rmt}$ for regular/chaotic spectra are obtained by averaging over the function values of 10 equidistant s over the width of the respective bins. Next the results for different numbers of bins $N_{bin} \in [15, 35]$ are renormalized, i.e. the reduced χ^2 given as χ^2 divided by the number of degrees of freedom $N_{bin} - 1$, which is appropriate to compare several data sets, is calculated and the minimum value taken as result

$$\chi^2_{red} = \min_{N_{bin} \in [15,35]} \left(\frac{\chi^2}{N_{bin} - 1}\right) \tag{16}$$

A number of different distributions which interpolate between the regular and chaotic limit of the nearest neighbor spacing distribution have been proposed and we use one of the popular distributions, the *Brody distribution* as an additional test for the transition between the limits. The *Brody distribution*, given by

$$P(s) = a(1 + \beta)s^\beta e^{-as^{\beta+1}} \quad ; \quad a = [\Gamma(\frac{2 + \beta}{1 + \beta})]^{\beta+1} \tag{17}$$

considers a power-law level repulsion and interpolates between the regular ($\beta = 0$) and chaotic ($\beta = 1$) limits [8].

To implement this test we take the middle points of the bins in s and the bin heights in P(s) as data points and fit the Brody distribution using Matlabs curve fitting tools with the *Trust-Region* algorithm. Analogous to the procedure for the χ^2 test we do this for an number of bins

$N_{bin} \in [15, 35]$ and take the outcome with best chi^2_{red} value for the fit as result for the parameter β in a given series of spacings.

While the nearest neighbor statistics deals with local correlations in the spectrum random matrix theory also makes predictions for functions characterizing the spectral correlations more globally. One of these functions, which we will utilize in our analysis is the *Number Variance* given as the variance $\Sigma^2(L)$ of the number of unfolded levels $N(\epsilon, \epsilon + L)$ in an interval $[\epsilon, \epsilon + L)]$, i.e.

$$\Sigma^2(L) = \langle [N(\epsilon, \epsilon + L) - L]^2 \rangle_\epsilon \tag{18}$$

since the average number of levels per unit of unfolded energy is equal to unity as result of the unfolding and with the average taken over all ϵ [17, 18]. Random matrix theory predicts a linear relation for the integrable Poissonian case and a logarithmic scaling for chaotic spectra:

$$\Sigma^2(L) = \begin{cases} L & \text{Poisson} \\ \frac{2}{\pi^2}[ln(2\pi L) + \gamma + 1 - \frac{\pi^2}{8}] + O(\frac{1}{L}) & \text{GOE} \end{cases} \tag{19}$$

where the parameter γ is the Euler constant $\gamma \approx 0.57722$.

For the numerical implementation the levels ϵ_i are obtained as the cumulative sum of spacings and $\Sigma^2(L)$ calculated by evaluating components $N(\epsilon, \epsilon + L) - L$ for discrete steps in ϵ and averaging over these components.

RESULTS

Since the dimension of the Hilbert space grows exponentially with an increasing number of lattice sites and particles , see equation (7), a numerical modeling and analysis is only practicable for small systems and fillings. The particle number is therefore generally chosen big enough to hold a statistically significant sample but small enough to be feasible considering the rapidly growing computation time for many of the needed calculations. To start our analysis we set the tunneling parameters J and J_d one leaving U as the only effective parameter which we varied in a range $[10^{-2}, 10^2]$ having found this range to cover the limits of weak interactions $J \gg U$ as well as the strong interaction regime $J \ll U$ as far as spectral statistics are concerned. We will consider 2x2, 2x3 and 3x3 systems starting out with 2x2 gradually going bigger and adding more diagonal couplings in order to study the effects of increasingly stronger coupled systems on the chaotic regime.

3.1 2X2-SYSTEMS

Figure 5 shows the performed χ^2 tests for the 2x2 systems with no, one and two diagonal couplings respectively and the inset figures in the topright corner show the parameter β obtained by the best fits with the Brody distribution as disussed in 2.3.2. The subsequent tabel 1 corresponds to the figures and holds the systemparameters as well as the minimum $log_{10}(\chi^2_{red})$ for the Possonian case (P) and the chaotic case (G) and the corresponding value of the parameter U.

The figures show features we have confirmed to be characteristic of the subsequently analyzed bigger systems as well.

For the cases $U = 0$ and $J = 0$ the Bose-Hubbard model is integrable [1] so as expected the plots show the nearest neighbor spacing distributions to correspont to the predictions for regular spectra in the limits of small and large U, i.e. level crossings dominate the spectra which shows in relatively small $log_{10}(\chi^2_{red})$ in testing the spectrum against the predictions for the Poissionian case and lage values for the chaotic case corresponding to the GOE. Around $U = J$ we see the
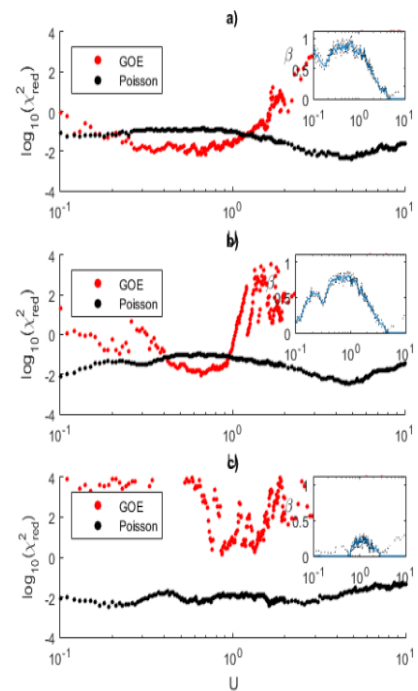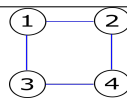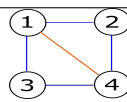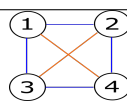

Figure 5: χ^2 tests and Brody parameter β for two by two lattices with no (a)), one (b)) and two (c)) diagonal couplings. Parameters and minumum values to be found in the corresponding subsequent table.

Table 1: Systemparameters and minimum $log_{10}(\chi^2_{red})$ for the Possonian case (P), chaotic case (G) with the corresponding values of the parameter U for the data displayed in fig. 5.

Plot	Sketch of the System	N	$min(\chi^2_{red}(P)$	$U(min(\chi^2_{red}(P)))$	$min(\chi^2_{red}(G)$	$U(min(\chi^2_{red}(G)))$
a)		20	-2.4141	4.9	-2.1845	0.63
b)		20	-2.4841	0.05	-2.0319	0.66
c)		20	-2.4522	0.19	3.5507	0.65

spectra of systems a) and b) transitioning into a regime with Wigener-Dyson distributed levelspacings as confirmed by the inset plots showing the parameter β where one can see a maximum in the region the χ^2 plots tell us that the spectrum is well described by the chaos-prediction. The dotted black lines show the 95% confidence bounds obtained in the fit.

We also see that the GOE distributed regime becomes smaller as an additional diagonal coupling is added in Plot b) and that there is no transition at all in the case of two diagonal couplings shown in Figure c). This is understandable considering that a mean-field approximation ensuing from a decoupling assumption $\hat{a}_i\hat{a}_j^\dagger \approx \langle\hat{a}_j^\dagger\rangle\hat{a}_i + \langle\hat{a}_j^\dagger\rangle\hat{a}_i - \langle\hat{a}_i\rangle\langle\hat{a}_j^\dagger\rangle$ with the expectation values in the ground state, is expected to work the better the higher the coordination number in the lattice i.e. the larger the spatial dimension and the more the sites are coupled with each other. This leads to a decomposition of the Hamitonian into a sum of on-site operators and a regular spectrum [4, 14]. As the table shows the best agreement with the GOE-predictions is found around $U \approx 0.6$ and the system a) gives the best, i.e. minimum value in $log_{10}(\chi^2_{red})$ for $U = 0.63$. The subsequent figures show the spacing distribution and the cumulative spacing distribution (insets) for this best case of a WD distributed spectrum in fig. 6 and the best regular case found in system b) in fig. 7 confirming the very good agreement with the predictions in the respective cases.
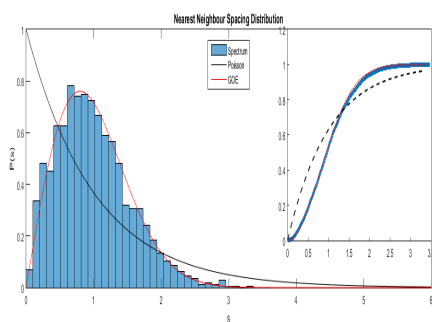

Figure 6: Nearest neighbor spacing distribution of the best chaotic case in 2x2 systems fond in system a) with $U = 0.63$
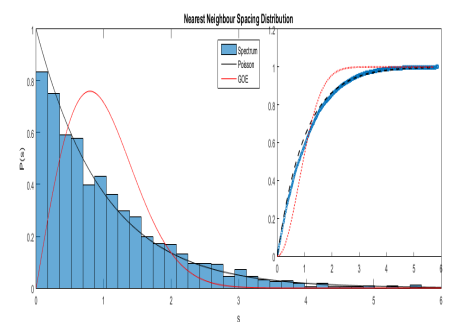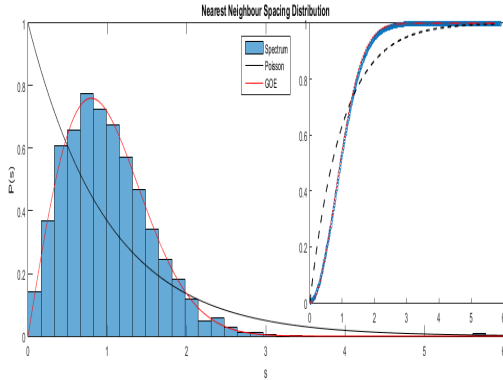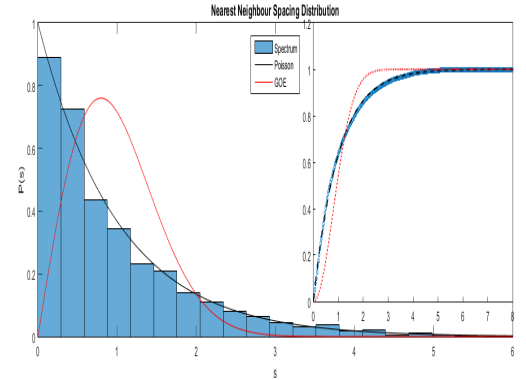

Figure 7: Nearest neighbor spacing distribution of the best regular case in 2x2 systems fond in system b) with $U = 0.05$

Turning our attention to bigger systems we see the same characteristics in figure 8 showing an analogous plot for the 2x3 case. Again we see the systems transitioning in and out of a regime with WD distributed levelspacings around $U \approx J$. Here however the narrowing of the regime with additional couplings does not happen as rapidly, i.e. gradually adding one diagonal coupling as is done in plots a)-e) only visibly decreases the range of parameters for which the spectra agree better with the predictions for chaotic systems than regular ones, when three additional couplings are added in figure d). Plot e) which corresponds to a fully diagonally coupled system still shows a narrow range of parameters where this is given and the relative χ^2_{red} values as well as the corresponding brody parameters indicate a mixed system which is better characterized by the chaos-predictions than the predictions for regular systems. Only as we introduce periodic boundary
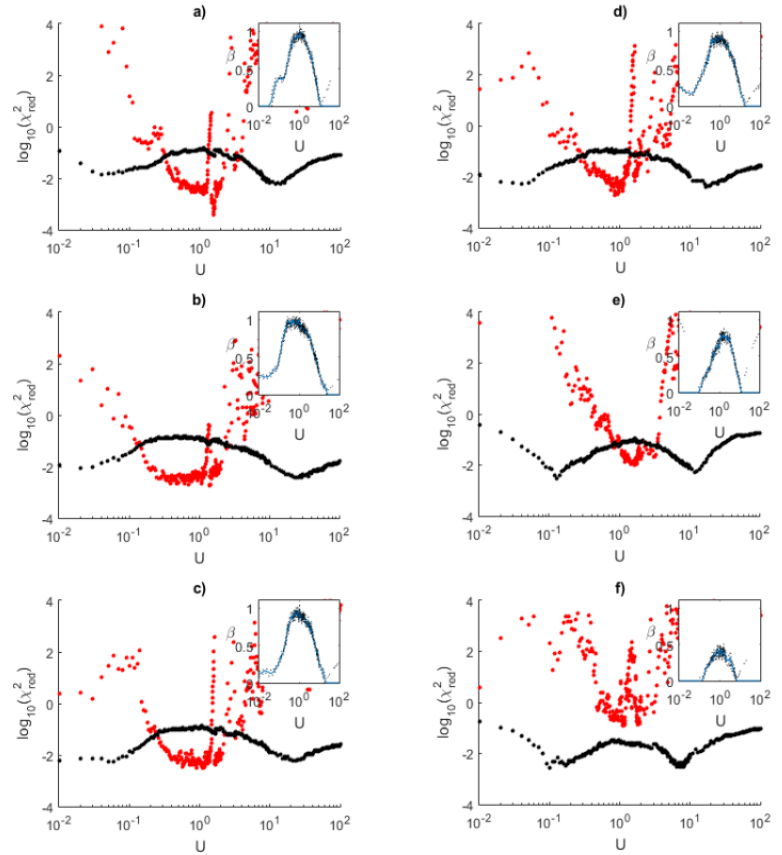
Figure 8: χ^2 tests and Brody parameter β for several 2x3 systems with different couplings. Parameters and minumum values to be found in the corresponding subsequent table.

conditions by coupling the system as shown in the table, the spectrum becomes regular for all values of U. Also apparent is that in comparison to the 2x2 systems the regime with WD distributed levelspacings has broadened and shifted to bigger values of U. This was expected as unit filling is generally favorable for chaotic behavior because the kinetic part and the interaction part of the Hamiltonian are of commensurable strength. In the limit $\frac{N}{L} \to 0$ the hopping term is dominant while in the opposite limit $\frac{N}{L} \to \infty$ the on-site interaction prevails. For the 2x2 systems we had filling $\frac{N}{L} = 5$ and here only $\frac{N}{L} \simeq 1.666$ therefore a broadening and wandering of the chaotic regime to bigger U was to be expected. However for the spectral statistics at different fillings to be comparable the dimension of the Hilbert space and corresponding number of spacings should be approximately the same and so far the dimension of the 2x2 systems with the considered parameters is $dim(\mathcal{H}(2x2)) = 1771$ and for the 2x3 systems we have $dim(\mathcal{H}(2x3)) = 3003$. Therefore the dimension of the 3x3 systems subsequently considered is chosen equal to the dimension in this 2x3 case to allow further comparison.

Table 2: Systemparameters and minimum $log_{10}(\chi^2_{red})$ for the Possonian case (P), chaotic case (G) with the corresponding values of the parameter U for the data displayed in fig. 8.

Plot	Sketch of the System	N	$min(\chi^2_{red}(P))$	$U(min(\chi^2_{red}(P)))$	$min(\chi^2_{red}(G))$	$U(min(\chi^2_{red}(G)))$
a)		10	-2.2393	12	-3.4154	1.57
b)		10	-2.4261	25	-2.7378	1.43
c)		10	-2.2412	0.06	-2.5095	0.92
d)		10	-2.4106	17	-2.744	0.86
e)		10	-2.5318	0.13	-1.9806	1.67
f)		10	-2.5625	0.1	-0.9281	1.15

The best chaotic case was found in system a) for $U = 1.57$ and the best agreement with predictions for regular systems in system f) for $U = 0.1$, the following plots show the corresponding distributions:

Figure 9: Nearest neighbor spacing distribution of the best chaotic case in 2x3 systems fond in system a) with $U = 1.57$

Figure 10: Nearest neighbor spacing distribution of the best regular case in 2x3 systems fond in system f) with $U = 0.1$

In the 3x3 systems investigated we generally find the same characteristics already discussed.

Here we consider a system with no diagonal couplings a) and two systems with four diagonal couplings in b) and c). While plot c) looks very similar to figure a) showing a broad chaotic regime, plot b) implies that the system transitions only into a mixed state for a narrow range of parameters. We believe this to be a consequence of the site in the middle of the system constituting a hub which strongly couples the adjacent sites. This strong coupling leads to a domination of the kinetic component, i.e. the hopping term is much stronger compared to system c) in the regime where c) shows WD distributed level spacings indicating chaos. In appendix A a figure showing the expectation value of the occupation number operator for the lattice site in the middle over time with initially all 6 particles in the middle is given. The comparatively strong fluctuations found in system b) illustrate the relatively strong kinetic contribution keeping the system from fully transitioning into chaos at this low filling of $\frac{N}{L} \simeq 0.666$. Interestingly in the fully diagonally coupled system d) where the particles are expected to be more evenly distributed again we see a broad chaotic regime again until in plot e) a kind of periodic boundary conditions are imposed and the spectrum becomes regular again in all U. As the filling is lower again and only $\frac{N}{L} \simeq 0.666$ we find that where present the chaotic regime even more shifted to bigger U and broadened in comparison to the 2x3 systems.
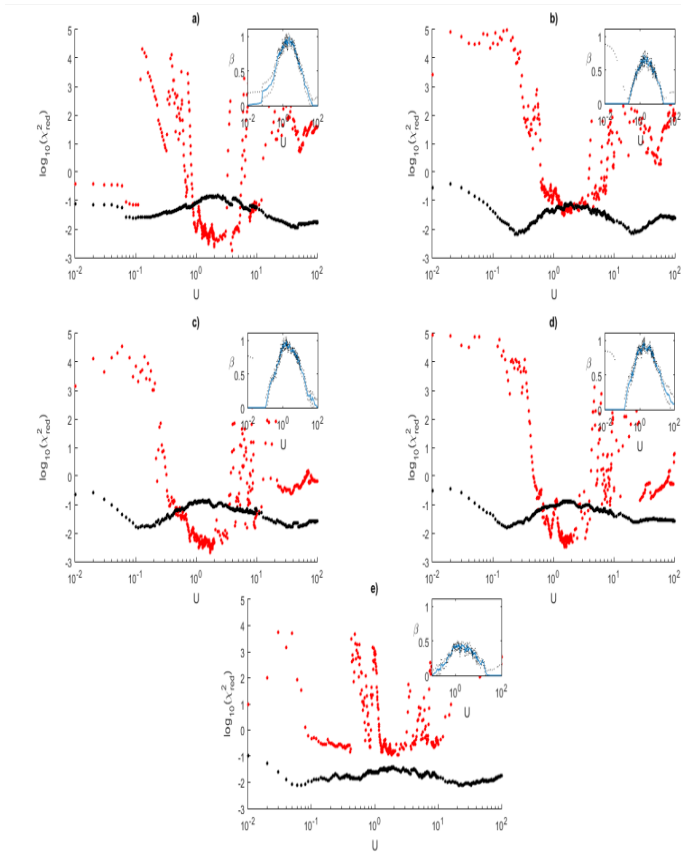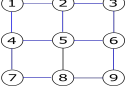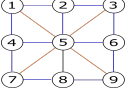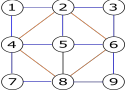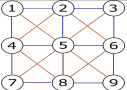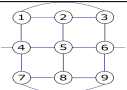

Figure 11: χ^2 tests and Brody parameter β for several 3x3 systems with different couplings. Parameters and minumum values to be found in the corresponding subsequent table.

Here we find the best chaotic case in sytem a) at $U = 3.9$ and the closest to regular case in system b) at $U = 0.25$ with the distributions depicted in the subsequent figures.

Table 3: Systemparameters and minimum $log_{10}(\chi^2_{red})$ for the Possonian case (P), chaotic case (G) with the corresponding values of the parameter U for the data displayed in fig. 11.

Plot	Sketch of the System	N	$min(\chi^2_{red}(P))$	$U(min(\chi^2_{red}(P)))$	$min(\chi^2_{red}(G))$	$U(min(\chi^2_{red}(G)))$
a)		6	-1.9637	48	-2.7583	3.9
b)		6	-2.1865	0.25	-1.522	1.47
c)		6	-1.8005	0.11	-2.6991	1.72
d)		6	-1.8016	0.17	-2.4997	1.54
e)		6	-2.1236	0.06	-0.9522	1.87
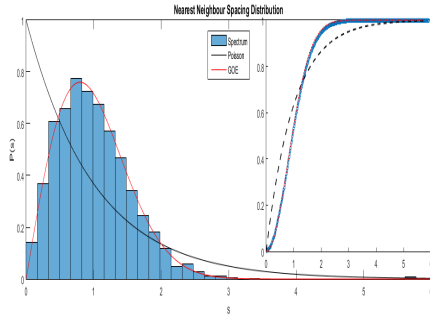
Figure 12: Nearest neighbor spacing distribution of the best chaotic case in 3x3 systems fond in system a) with $U = 3.9$
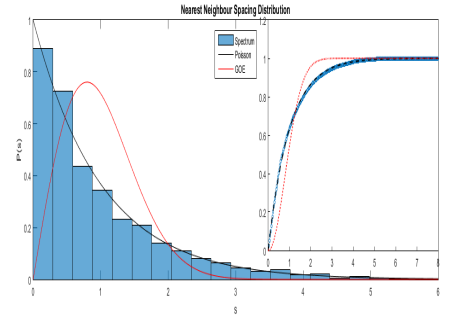
Figure 13: Nearest neighbor spacing distribution of the best regular case in 3x3 systems foud in system b) with $U = 0.25$

3.4 $J_D \neq J$

To study the effect of changing the parameter J_d we made some additional calculations with $J_d = \frac{1}{\sqrt{2}}$. Figure 14 shows the results for three systems we already discussed with $J_d = J = 1$. In comparing these figures to the corresponding figures above we note very slight shift and narrowing of the chaotic regime to smaller U. This is expected and consistent since the systems are not coupled as strongly as before and off diagonal elements in the Hamiltonian-Matrix corresponding to diagonally coupled states are relatively lowered in value. Therefore qualitatively similar behavior should be expected for lower values in U.
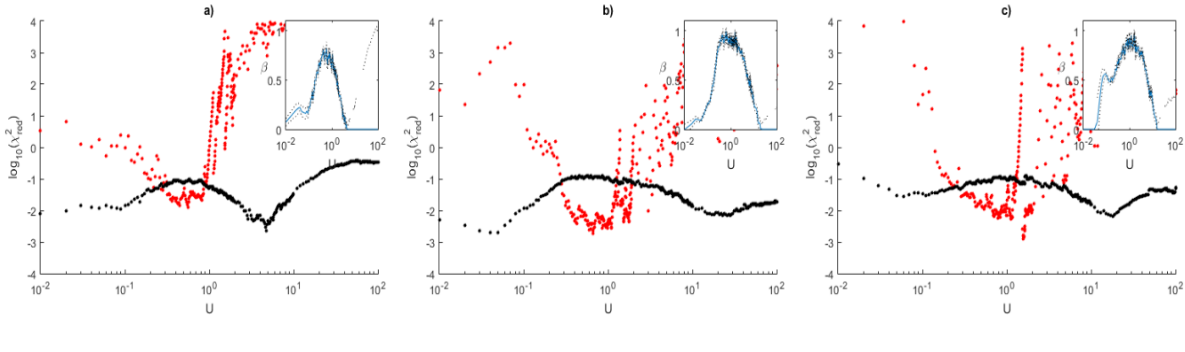
Figure 14: χ^2 tests and Brody parameter β with $J_d = \frac{1}{\sqrt{2}}$, figure a) corresponding to plot b) in fig. 5, b) to c) in fig. 8 and c) to d) in fig. 8

3.5 Σ^2-STATISTICS

Finally we consider the spectral correlations more globally by means of the discussed Σ^2-Test, see 2.3.2, for the best cases identified in the respective series of considered systems. As the figure 15 shows the long range spectral correlations follow the predictions for the respective cases usually only for a short range. For the chaotic cases on the left we find the best agreement for the 2x2 systems up to about $L = 5$ and increasingly shorter ranges of good agreement for the bigger systems. For the regular cases the opposite is given and we find the spectral data of the 3x3 case to fit the predictions best and up to a scale of about $L = 4$.

As L grows larger logarithmic scaling generally prevails and we can see the onset of oscillations in the number variance. These results do not fit the previous results using measures of the local fluctuations very well and there seems to be no correlation between the obtained best $log_{10}\chi^2_{red}$ values and the range of good agreement in these Σ^2 statistics. While the short range correlations have been found to have very little sensitivity to the unfolding procedure many studies show the long range correlation functions to be highly sensitive in that regard. We have not tried to apply conceptually different unfolding methods but were able to confirm this sensitivity by varying the window size w (see 2.3.1) used in the unfolding [2, 9]. With this in mind we think it possible that more sophisticated unfolding techniques lead to a much better agreement with the expected scaling.
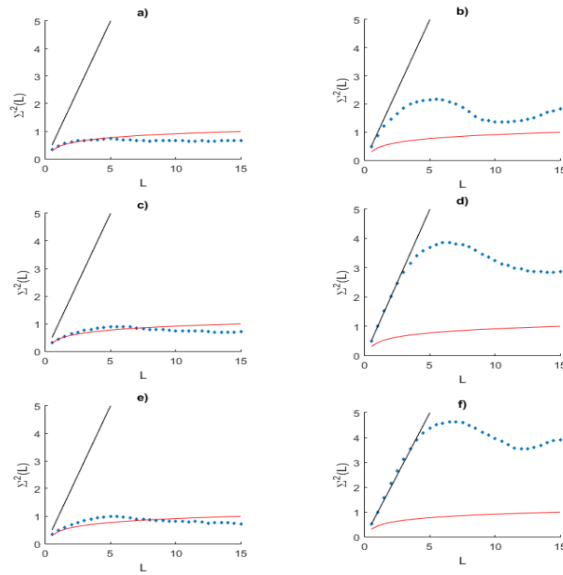

Figure 15: Σ^2 tests for the best regular/chaotic cases identified for the 2x2 systems a),b), the 2x3 systems c),d) and the 3x3 systems e),f). Levels obtained via local unfolding with $w = 6$.

CONCLUSION AND PERSPECTIVES

4

In this project we performed a numerical study of the spectra of the Bose-Hubbard Hamiltonian on small 2-dimensional lattices. It was shown that several characteristics found in 1-dimensional systems are present in the studied systems as well. We initially set the hopping parameter for nearest neighbor and diagonally coupled lattice sites to unity leaving the on-site interaction parameter U as only effective parameter and confirmed that the spectra are regular in the limits of weak and strong interactions. For systems coupled not too strongly a nonintegrable regime with Wigner-Dyson distributed level spacings can be found in the vicinity of equal interaction- and hopping-parameters $U = J$. In going to bigger systems with lower fillings down to filling 0.666 we have shown this regime to broaden and shift to bigger values of U. Intoducing more and more couplings to the systems generally leads to smaller WD distributed regimes but the exact structure needs to be considered. This is apparent in an example of two 3x3 systems considered with the same number of diagonal couplings distributed in different manners showing very different distributions of nearest neighbor level spacings in the interesting regime around $U = J$. Introducing a kind of periodic boundary conditions was observed to lead to regular spectra for all parameters in all considered systems and fillings. For the spectral correlations on a longer scale, namely the Σ^2 statistics, we found the agreement with cases identified as having a Poisson or WD distributed nearest neighbor spacing distribution in good approximation to hold only up to a medium energy scale of maximally $L = 5$ if at all. But reviewing this with more sophisticated methods of unfolding would be very interesting as the number variance is highly sensitive to the unfolding method employed and a more general approach might show the correlations to resemble the expected scaling much better and on a larger energy scale. To put it in a nutshell we have shown the existence of a regime with WD distributed nearest neighbor level spacings for a systems as big as 3x3 provided the system is not too strongly coupled and low filling factors of order unity, giving strong indications of chaotic behavior. These results may provide a stepping stone for further statistical inquiries such as investigating the dependence on the filling factor more thoroughly or using different measures for quantum chaos to guarantee that the spectra in the identified regimes with WD distributed level spacings has the universal statistical properties associated with quantum chaos. In addressing this problem form a dynamic point of view one might also be aided by the findings as they provide a reference and starting point in pinpointing the interesting regimes.

Part III

APPENDIX

COMPARISON OF THE 3X3 SYSTEMS B) AND C)

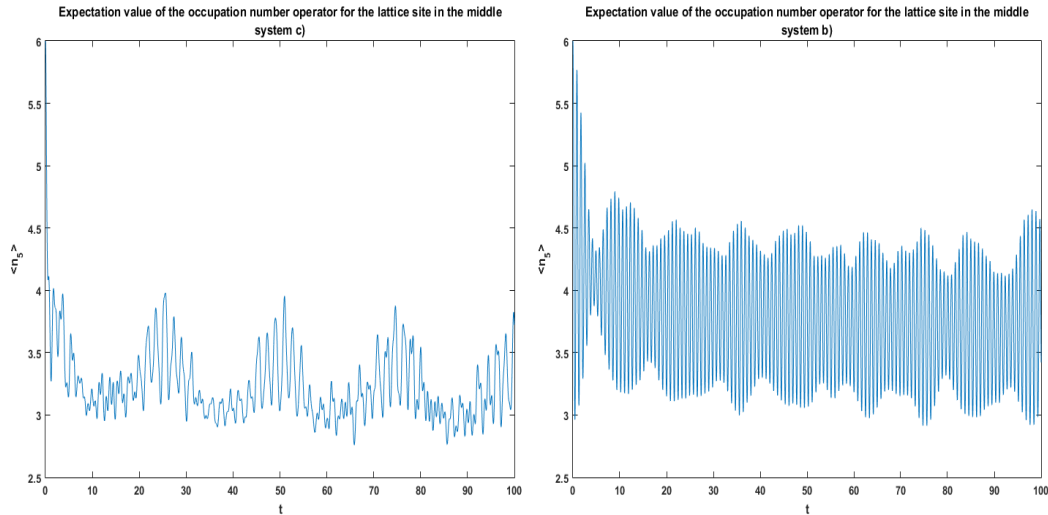The following figure shows the expectation values of the occupation number operator for the lattice site in the middle for systems b) and c) over time. They were obtained by integrating the Schrödinger equation using Matlabs *ode45* algorithm. We set $\hbar = 1$, integrated for a timespan [0,100] and used the resulting coefficients at times t to calculate the expectation value of the occupation number operator for the lattice site in the middle of the 3x3 systems in question b) and c).

Figure 16: Expectation value of the occupation number operator for the lattice site in the middle for systems b) and c) over time

The figures show that in system b) the expectation value fluctiates very rapidly in contrast to the result for system c) indicating a lot of tunneling in system b) compared to system c) with the less strongly coupled well.

REFERENCES

[1] A. R. Kolovsky and A. Buchleitner. Quantum chaos in the bose-hubbard model. *Europhys. Lett.*, 68(5):632–638, 2004. doi: 10.1209/epl/i2004-10265-7. URL http://dx.doi.org/10.1209/epl/i2004-10265-7.

[2] Ashraf A. Abul-Magd and Adel Y. Abul-Magd. Unfolding of the Spectrum for Chaotic and Mixed Systems. Physica A 396 (2014) 185-194, 2013. arXiv:1311.2419v1.

[3] Immanuel Bloch, Jean Dalibard, and Wilhelm Zwerger. Many-body physics with ultracold gases. *Rev. Mod. Phys.*, 80:885–964, Jul 2008. doi: 10.1103/RevModPhys.80.885. URL http://link.aps.org/doi/10.1103/RevModPhys.80.885.

[4] P. Buonsante and A. Vezzani. Ground-state fidelity and bipartite entanglement in the bose-hubbard model. *Phys. Rev. Lett.*, 98:110601, Mar 2007. doi: 10.1103/PhysRevLett.98.110601. URL http://link.aps.org/doi/10.1103/PhysRevLett.98.110601.

[5] Pierfrancesco Buonsante and Sandro Wimberger. Engineering many-body quantum dynamics by disorder. *Phys. Rev. A*, 77:041606, Apr 2008. doi: 10.1103/PhysRevA.77.041606. URL http://link.aps.org/doi/10.1103/PhysRevA.77.041606.

[6] Giulio [Hrsg.] Casati, editor. *Quantum chaos*. Cambridge Univ. Press, Cambridge, 1995. ISBN 0-521-43291-X ; 978-0-521-43291-7.

[7] Matthew P. A. Fisher, Peter B. Weichman, G. Grinstein, and Daniel S. Fisher. Boson localization and the superfluid-insulator transition. *Phys. Rev. B*, 40:546–570, Jul 1989. doi: 10.1103/PhysRevB.40.546. URL http://link.aps.org/doi/10.1103/PhysRevB.40.546.

[8] K Ganesan and M Lakshmanan. Applicability of brody distribution in the study of quantum chaos of the hydrogen atom in a generalized van der waals potential. *Journal of Physics B: Atomic, Molecular and Optical Physics*, 27(13):2809, 1994. URL http://stacks.iop.org/0953-4075/27/i=13/a=011.

[9] J. M. G. Gómez, R. A. Molina, A. Relaño, and J. Retamosa. Misleading signatures of quantum chaos. *Phys. Rev. E*, 66:036209, Sep 2002. doi: 10.1103/PhysRevE.66.036209. URL http://link.aps.org/doi/10.1103/PhysRevE.66.036209.

[10] J. Hubbard. Electron correlations in narrow energy bands. *Proceedings of the Royal Society of London. Series A, Mathematical and Physical Sciences*, 276(1365):pp. 238–257, 1963. ISSN 00804630. URL http://www.jstor.org/stable/2414761.

[11] D. Jaksch, C. Bruder, J. I. Cirac, C. W. Gardiner, and P. Zoller. Cold bosonic atoms in optical lattices. *Phys. Rev. Lett.*, 81:3108–3111, Oct 1998. doi: 10.1103/PhysRevLett.81.3108. URL http://link.aps.org/doi/10.1103/PhysRevLett.81.3108.

[12] M. L. Mehta. *Random matrices*. Pure and applied mathematics ; v. 142. Elsevier/Academic Press, Amsterdam ; San Diego, CA, 3rd ed edition, 2004. ISBN 0-12-088409-7 ; 978-0-12-088409-4. URL http://www.ub.uni-heidelberg.de/cgi-bin/edok?dok=http%3A%2F%2Fwww.engineeringvillage.com%2Fcontroller%2Fservlet%2FOpenURL%3Fgenre%3Dbook%26isbn%3D9780120884094. Includes bibliographical references (p. 655-679) and indexes.

[13] Jun J. Sakurai and Jim Napolitano. *Modern quantum mechanics*. Always learning. Pearson, Harlow, 2. ed., new internat. ed. edition, 2014. ISBN 1-292-02410-0 ; 978-1-292-02410-3.

[14] K. Sheshadri, H. R. Krishnamurthy, R. Pandit, and T. V. Ramakrishnan. Superfluid and insulating phases in an interacting-boson model: Mean-field theory and the rpa. *EPL (Europhysics Letters)*, 22 (4):257, 1993. URL http://stacks.iop.org/0295-5075/22/i=4/a=004.

[15] Hans-Jürgen Stöckmann. *Quantum chaos*. Cambridge Univ. Press, Cambridge [u.a.], 1. pbk. version (with corrections) edition, 2006. ISBN 0-521-59284-4 ; 0-521-02715-2 ; 978-0-521-59284-0 ; 978-0-521-02715-1.

[16] Andrea Tomadin, Riccardo Mannella, and Sandro Wimberger. Many-body interband tunneling as a witness of complex dynamics in the bose-hubbard model. *Phys. Rev. Lett.*, 98:130402, Mar 2007. doi: 10.1103/PhysRevLett.98.130402. URL http://link.aps.org/doi/10.1103/PhysRevLett.98.130402.

[17] Andrea Tomadin, Riccardo Mannella, and Sandro Wimberger. Many-body landau-zener tunneling in the bose-hubbard model. *Phys. Rev. A*, 77:013606, Jan 2008. doi: 10.1103/PhysRevA.77.013606. URL http://link.aps.org/doi/10.1103/PhysRevA.77.013606.

[18] Sandro Marcel Wimberger. *Nonlinear dynamics and quantum chaos*. Graduate Texts in Physics. Springer, Cham ; Heidelberg [u.a.], 2014. ISBN 978-3-319-06342-3 ; 978-3-319-06343-0.

LIST OF FIGURES

Ich versichere, dass ich diese Arbeit selbstständig verfasst und keine anderen als die angegebenen Quellen und Hilfsmittel benutzt habe.

Heidelberg, den 13.7.2015,

(Darius Hoffmann)